the normal distribution using the transformation $\ln(x/(1-x))$, where x is the relative spectral power (Gasser et al., 1982). To reduce the number of variables used for classification, we averaged band power values over all 21 channels.

Linear discriminant analysis (LDA) (using publicly available software for both linear classical and robust discriminant analysis, by Croux and Dehon, 2001) was used for discriminating MCI and control groups on the basis of log-transformed relative spectral power in the six frequency bands, averaged over channels. To improve validation of the classification results, discriminant analysis was applied in combination with jack-knifing, a procedure which typically produces lower discrimination rate than, e.g. cross-validation based on using part of a sample for learning and other part for classification, but is statistically more correct and enables increased reproducibility in other samples (Besthorn et al., 1997). Jack-knifing means that each case is classified using individual discriminant function trained with all cases except this one. Results of this procedure was used for computing sensitivity (the number of MCI subjects who were classified as MCI divided by the number of all subjects in MCI group) and specificity (the number of normal subjects who were classified as normal divided by number of all normal subjects).

3. Results

Averaged power spectra of each AMUSE component for patients and control subjects are presented in Fig. 2. As expected, components with lower indices (corresponding to higher linear predictability) had higher relative power at lower frequencies, while components with higher indices had higher relative power at highest frequencies. What is especially important is that the difference between patients and control subjects was clearer in the components with lower indices (i.e. components with highest linear predictability and highest variance of their projections). Thus, in further analysis we used combination of components with lowest indices.

To estimate how many components with highest linear predictability provides optimal classification rate, we applied LDA without jack-knifing (the latter requires much more computation time) to all projected components with indices from 1 to 2, from 1 to 3 and so on. Overall misclassification rate was computed each time by applying obtained discriminant function to the same 60 subjects (22 patients+38 controls). Results are presented in Fig. 3. The best classification was obtained for projection of the first five components (with indices from 1 to 5); however, performance was also high when the number of components

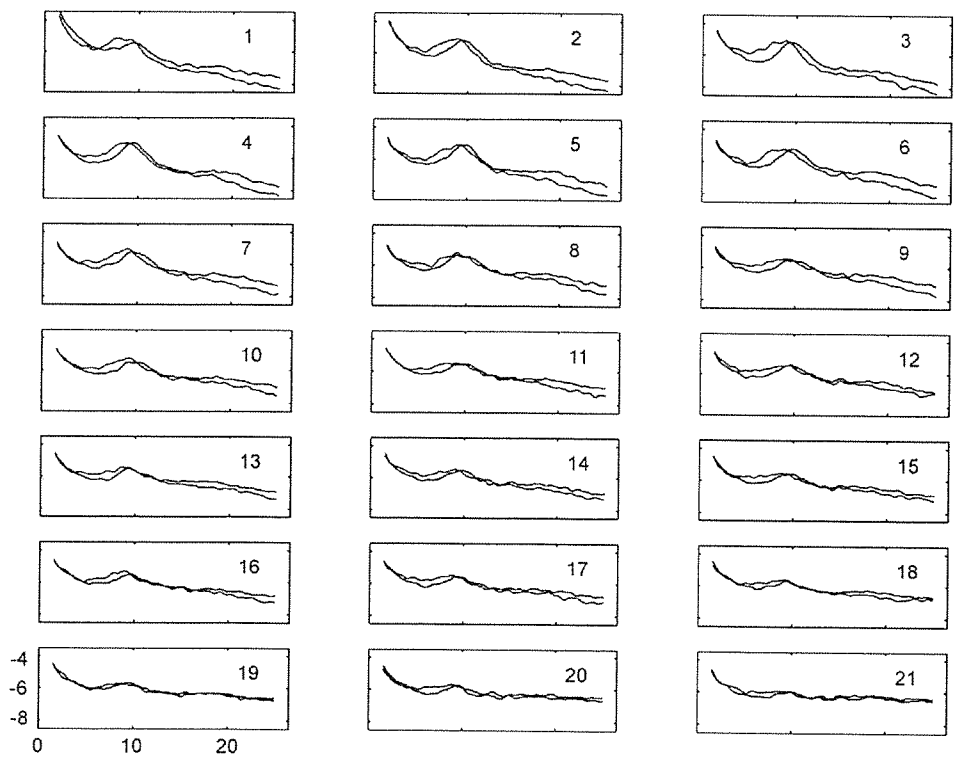

Fig. 2. Averaged power spectra of AMUSE components 1–21. x-axis: frequency, Hz. y-axis: transformed relative spectral power. Relative spectral power was obtained by dividing the absolute values in each frequency bin by total power in the range 1.5–25 Hz. Before averaging, the power values were normalized using transformation $\log(x/(1-x))$ (negative values appear because of this transformation). Red: MCI patients later progressed to AD ($n=22$). Black: control subjects ($n=38$).

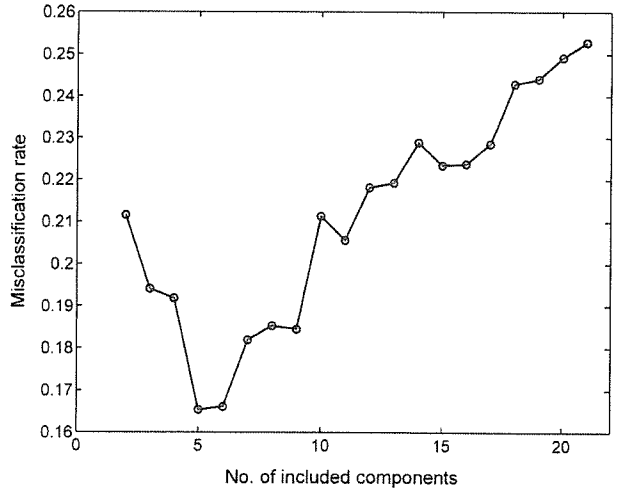

Fig. 3. LDA approximate (computed without cross-validation) misclassification rate for different number of projected components. Only components with highest linear predictability were used, thus, data points correspond to the following combinations of components: 1,2; 1–3; 1–4;...1–20; 1–21.

was in a rather wide range between 3 and 9. Thus, the method appeared to be robust in respect to the number of selected components.

Classification with jack-knifing procedure was applied to projections of several combinations of components, including 1–5 which appeared to be optimal according to Fig. 3. As follows from Table 1, results of classification were better if preprocessing included selection of AMUSE components with lower indices (1–5, 1–7, 1–10), comparing to raw data. When components with higher indices (6–21, 8–21, 11–21) were selected in preprocessing, the results were worse than in the case of raw data. Best results were obtained with components 1–5 and 1–7 (improvement by 14% over the raw data for classification of MCI and by 8% for control subjects), while components 11–21 gave the worst results. More detailed classification results for two combinations of components (1–5 and 1–10) and for the raw data, presented as Relative Operating Characteristic (ROC) curves in Fig. 4, confirm that use of components 1–10 only slightly improved the classification (Fig. 4(a)), while improvement of classification with components 1–5 over raw data was substantial (Fig. 4(b)). Best classification performance after preprocessing using 1–5 components was obtained in the range of approximately 0.6–0.8 for sensitivity and 0.7–0.9 for specificity. Selection of components with high indices was clearly not good for classification: for components 11–21 classification performance was almost at random level (Fig. 4(a)).

Table 1
Number of subjects who were correctly and incorrectly classified by discriminant analysis applied to relative power in six frequency bands after selection and back projection of certain AMUSE components (AMUSE filtering). Results were obtained using jack-knifing

AMUSE components selected in preprocessing	Misclassified		Correctly classified %		
	MCI $n=22$	Controls $n=38$	MCI $n=22$	Controls $n=38$	All $n=60$
No preprocessing	9	9	59	76	70
Components 1–5	**6**	**6**	**73**	**84**	**80**
Components 1–7	**6**	**6**	**73**	**84**	**80**
Components 1–10	6	9	73	76	75
Components 6–21	9	11	59	71	67
Components 8–21	9	11	59	71	67
Components 11–21	**12**	**12**	**45**	**68**	**60**

4. Discussion

With EEG preprocessing proposed in this paper, we obtained 80% rate of correct classification (Table 1) for MCI using only 20 s artifact-free interval of EEG recording from each patient or control subject. While groups of patients and controls were relatively small (22 and 38, correspondingly), it should be noted that the classification performance was estimated using the rigorous jack-knifing cross-validation procedure, which reduce the risk of overstating the results. The jack-knifing procedure was applied only to LDA but not to approximate optimization of the choice of components for back projection. Optimization of the choice of components was made for the whole dataset on the basis of components' spectra and preliminary run of LDA. Nevertheless, Figs. 2 and 3 suggest that the dependence of the difference between patients' and controls' spectra on component index and dependence of LDA results on the number of selected components were systematic; thus, it is unlikely that we simply picked up some random variations in LDA performance dependent on details of preprocessing and that improvement of LDA performance by preprocessing with the same parameters will be not reproducible in other groups of patients and controls.

The procedure of selection of artifact-free EEG intervals used in this study could introduce some bias in absolute values of discrimination results, because it was done by only one expert, and this expert did know to which group each EEG belongs. In fact, the proportion of the EEG recordings which were not analyzed due to the lack of a sufficiently long artifact-free interval was different in the groups of patients (12%) and controls (19%), and this difference was in the direction which can be expected if the criteria for selecting the analyzed interval were more strict for control group. This difference could be a result of random variations, and it should be noted that most of artifacts were easily identifiable (due to low amplifier range, any high amplitude artifact led to amplifier saturation), so it was rather unlikely that the subjective bias could strongly

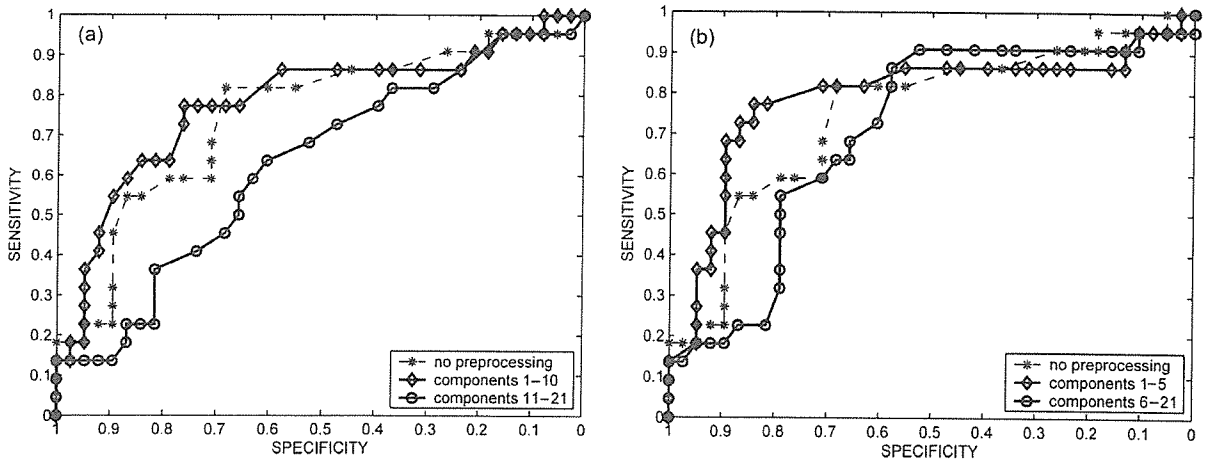

Fig. 4. Relative Operating Characteristic (ROC) curves obtained using jack-knifing for classification of MCI patients later progressed to AD ($n=22$) versus normal controls ($n=38$). LDA was applied to relative power in six EEG frequency bands. Comparison between data without preprocessing and data after selection and back projection of certain AMUSE components (AMUSE filtering). (a) Selection of first 10 components, compared to the rest of components and no preprocessing. (b) Selection of first five components, compared to the rest of components and no preprocessing.

influence the results. However, we cannot guarantee that the use of subjective criteria for selection of artifact free intervals did not affect classification results at all, and it is difficult to predict whether the obtained high values of specificity and sensitivity can be reproduced in other studies. We would like to emphasize, nevertheless, that our main claim is that the proposed preprocessing method increases the performance *relatively* to the level obtained without its use. This tendency could not be altered by subjective bias in search for artifact-free intervals.

We do not discuss here to which physiologically meaningful brain sources AMUSE components can correspond, because they can be a mixture of activity from many physical sources in the brain. This is clearly not critical for improving of EEG classification. The improvement of classification after AMUSE filtering comparing to non-preprocessed EEG data was probably caused by higher difference between patients' and controls' spectra in the selected components than in the non-used (filtered off) components. Spectra computed for AMUSE components separated by BSS algorithm AMUSE (Fig. 2) demonstrate that the difference between patients and controls decreased with the index of component. Interestingly, this effect is visible at the same time in several frequency ranges: in theta range, where patients had an increase of relative power; in alpha range, where shift of the peak to slower frequencies was observed in patients; and in beta range, where relative power was lower for patients. All these differences in spectral power are typically found between AD patients and normal subjects. Spectra of components with the highest indices showed almost no difference between patients and controls, and it was not surprising that the performance of classification based on back projection of only these components was close to random level (Fig. 4(a), components 11–21). Thus, AMUSE components with higher indices can be considered as mainly representing 'noise' which makes difficult, in processing of raw EEG, to detect diagnostically important changes in characteristics of 'signal'. Note that 'signal' and 'noise' here are not labels for signal from brain sources and for artifacts: we refer to the 'signal' only as to diagnostically important (significant) part (subspace) of raw EEG signal, and to 'noise' as to the diagnostically not important part (non-significant subspace). AMUSE filtering, i.e. extraction of part of EEG reach with 'signal' by using only 'best' (here, most useful for diagnosis) components for back projection, naturally leads to the improvement of 'signal-to-noise ratio' and, as a result, to the improvement of EEG classification.

A BSS-based approach to improvement of signal-to-noise ratio in MEG signal by defining and removing noise subspace was already developed (Kawakatsu, 2003). More simple and already rather widely used technique is removing EEG and MEG artifact-related components with BSS using visual or automatic identification of such components one by one after decomposition (e.g. Jung et al., 2000). However, since in many kinds of EEG and MEG studies the goal is to extract the brain signal in possibly less distorted form, the existing techniques are limited to remove only such part of raw signal, which contain no or almost no components of brain origin but rather external artifacts and noise. In EEG classification tasks, such as diagnosis or Brain-Computer Interface (BCI), preserving the original signal is less important, noise can be defined not only as artifacts but also as any part of the signal which do not contribute to the difference between the classes of EEG which should be differentiated, and larger subspace with high percentage of such 'noise' can be removed. The existing techniques can only identify, by some a priori known characteristics, noise components (Barbati et al., 2004; Jung et al., 2000; Kawakatsu, 2003)

and some very specific diagnostically important components (epileptic spike separation: e.g. Kobayashi et al., 2002). Xu et al. (2004) recently suggested using a subspace approach for differentiating between task-related EEG patterns in BCI. They selected several ICA components related to P300 according to the a priori knowledge of P300 spatio-temporal pattern and reconstructed a clear P300 peak using back projection of these components. Like in the case of epileptic spikes, the components in this case were easily identifiable.

In a general case, however, significant and non-significant components are not easily identifiable. The task becomes especially challenging if EEG components from different subjects should be compared, because the sets of components produced by BSS in different subjects usually differ dramatically. In our approach, we rank components using some empirical rule, such as their linear predictability, and select those where difference between the pathological and normal EEG is most differentiated. This made possible to achieve substantial improvement in the discrimination between MCI patients who later progressed to AD and normal age-matched controls. To our best knowledge, no study till now investigated the application of BSS/ICA methods as preprocessing tools with possible application for AD diagnosis.

Dividing of components into two groups (or subspaces) as below or above some component's index (in the case of ranking) or using a threshold for some index computed for each component is not the only way. One may try to divide the sets of components at more than one level and, e.g. remove not only components with highest indices but also with the lowest indices. As one may suppose from Fig. 1(b) (example of individual data), the first two components could represent, to rather high extent, artifacts (roving eye movements). Fig. 2, however, shows that components #1 and #2 substantially differed between groups. We made an attempt to exclude 1 or 2 first components from the analysis and this, in fact, led to slightly lower discrimination results. However, it is possible that for other data (for example, including high amplitude low frequency artifacts) or other processing techniques dividing the set of components on more than one level could be beneficial.

Not only spectral but also other EEG features, such as measures of synchronization between channels, can be investigated for the possibility of improving contrast between pathological and normal data using the presented approach. Several studies indicated that synchronization between different brain areas is sensitive to AD. Such results were obtained for quite different techniques, including coherence (e.g. Adler et al., 2003; Jelic et al., 1996; Locatelli et al., 1998; Wada et al., 1998), mutual information (Jeong et al., 2001) and synchronization likelihood (a new measure combining estimation of linear and nonlinear coupling) (Stam et al., 2003). One may hypothesize that EEG components can be divided into two parts, one of which represents signal subspace with lower (or stronger) synchronization among some cortical areas in AD relative to normal EEG, and another one represents signal subspace which synchronization characteristics are not related to the disease. In this case, the general approach described in this paper also could appear to be useful. One may probably try to apply it also in the case of using nonlinear measures (see review in Jeong, 2004) or in combination with other advanced approaches.

There is obviously room for improvement and extension of the proposed method both in ranking and selection of optimal (significant) components, apparatus and post-processing to perform classification task. Especially, we can apply a wide variety of BSS methods, i.e. instead of the applied and investigated second order statistics spatio-temporal decorrelation, we can exploit other new types of BSS algorithms, such as higher order statistic ICA, sparse component analysis or smooth component analysis with a suitably ordered and ranked components. Furthermore, instead of standard LDA we can use more sensitive and robust methods, such as neural networks or support vector machine (SVM) classifiers. Classification can be probably strongly improved by supplementing the set of spectral power values which we used with much different indices, such as alpha dipolarity, a new index depending on prevalence local vs. distributed sources of EEG alpha activity, which was shown to be very sensitive to AD-related cortical impairment (Musha et al., 2002). Additional attractive but still open issue is that using the proposed approach, we can not only detect but also measure in consistent way the progression of AD and influence of medications. The proposed method can also be potentially useful and effective tool for differential diagnosis of AD from other types of dementia, and possibly for diagnosis of other diseases. Other areas of EEG analysis can be also possible field for the application of our preprocessing technique. For these purposes, more studies would be needed to asses of the impact of the proposed enhancement/filtering procedures on the EEG signal of interest.

References

Adler G, Brassen S, Jajcevic A. EEG coherence in Alzheimer's dementia. J Neural Transm 2003;110(9):1051–8.

Barbati G, Porcaro C, Zappasodi F, Rossini PM, Tecchio F. Optimization of an independent component analysis approach for artifact identification and removal in magnetoencephalographic signals. Clin Neurophysiol 2004;115(5):1220–32.

Belouchrani A, Abed-Meraim K, Cardoso JF, Moulines E. A blind source separation technique using second order statistics. IEEE Trans Signal Process 1997;45(2):434–44.

Besthorn C, Zerfass R, Geiger-Kabisch C, Sattel H, Daniel S, Schreiter-Gasser U, et al. Discrimination of Alzheimer's disease and normal aging by EEG data. Electroencephalogr Clin Neurophysiol 1997; 103(2):241–8.

Blennow K, Hampel H. CSF markers for incipient Alzheimer's disease. Lancet Neurol 2003;2(10):605–13.

Cichocki A, Amari S. Adaptive blind signal and image processing: learning algorithms and applications. New York, NY: Wiley; 2003.

Cichocki A, Amari S, Siwek K, Tanaka T, et al. ICALAB toolboxes. [Available online at http://www.bsp.brain.riken.jp/ICALAB]

Croux C, Dehon C. Software package for robust discriminant analysis; 2001. [http://www.econ.kuleuven.ac.be/public/NDBAE06/software/DA/matlab.htm]

DeKosky ST, Marek K. Looking backward to move forward: early detection of neurodegenerative disorders. Science 2003;302(5646): 830–4.

Delorme A, Makeig S. EEGLAB: an open source toolbox for analysis of single-trial EEG dynamics including independent component analysis. J Neurosci Methods 2004;134(1):9–21.

Gasser T, Bacher P, Mocks J. Transformations towards the normal distribution of broad band spectral parameters of the EEG. Electroencephalogr Clin Neurophysiol 1982;53(1):119–24.

Goncharova II, McFarland DJ, Vaughan TM, Wolpaw JR. EMG contamination of EEG: spectral and topographical characteristics. Clin Neurophysiol 2003;114(9):1580–93.

Hara J, Shankle WR, Musha T. Cortical atrophy in Alzheimer's disease unmasks electrically silent sulci and lowers EEG dipolarity. IEEE Trans Biomed Eng 1999;46(8):905–10.

Hodges JR. Cognitive assessment for clinicians. Oxford: Oxford Medical Publications; 1993 p. 197–228.

Huang C, Wahlund L, Dierks T, Julin P, Winblad B, Jelic V. Discrimination of Alzheimer's disease and mild cognitive impairment by equivalent EEG sources: a cross-sectional and longitudinal study. Clin Neurophysiol 2000;111(11):1961–7.

Jelic V, Shigeta M, Julin P, Almkvist O, Winblad B, Wahlund LO. Quantitative electroencephalography power and coherence in Alzheimer's disease and mild cognitive impairment. Dementia 1996;7(6): 314–23.

Jeong J. EEG dynamics in patients with Alzheimer's disease. Clin Neurophysiol 2004;115(7):1490–505.

Jeong J, Gore JC, Peterson BS. Mutual information analysis of the EEG in patients with Alzheimer's disease. Clin Neurophysiol 2001;112(5): 827–35.

Joyce CA, Gorodnitsky IF, Kutas M. Automatic removal of eye movement and blink artifacts from EEG data using blind component separation. Psychophysiology 2004;41(2):313–25.

Jung TP, Makeig S, Westerfield M, Townsend J, Courchesne E, Sejnowski TJ. Removal of eye activity artifacts from visual event-related potentials in normal and clinical subjects. Clin Neurophysiol 2000;111(10):1745–58.

Kawakatsu M. Application of ICA to MEG noise reduction. Fourth international symposium on independent component analysis and blind signal separation (ICA2003), Nara, Japan; April 1–4, 2003, p. 535–41.

Kobayashi K, Akiyama T, Nakahori T, Yoshinaga H, Gotman J. Systematic source estimation of spikes by a combination of independent component analysis and RAP-MUSIC. II: preliminary clinical application. Clin Neurophysiol 2002;113(5):725–34.

Locatelli T, Cursi M, Liberati D, Franceschi M, Comi G. EEG coherence in Alzheimer's disease. Electroencephalogr Clin Neurophysiol 1998; 106(3):229–37.

McKhann G, Drachman D, Folstein M, Katzman R, Price D, Stadlan EM. Clinical diagnosis of Alzheimer's disease: report of the NINCDS-ADRDA Work Group under the auspices of Department of Health and Human Services Task Force on Alzheimer's Disease. Neurology 1984; 34(7):939–44.

Musha T, Asada T, Yamashita F, Kinoshita T, Chen Z, Matsuda H, et al. A new EEG method for estimating cortical neuronal impairment that is sensitive to early stage Alzheimer's disease. Clin Neurophysiol 2002; 113(7):1052–8.

Petersen RC, editor. Mild cognitive impairment: aging to Alzheimer's Disease. New York: Oxford University Press. 2003.

Pritchard WS, Duke DW, Coburn KL, Moore NC, Tucker KA, Jann MW, et al. EEG-based, neural-net predictive classification of Alzheimer's disease versus control subjects is augmented by non-linear EEG measures. Electroencephalogr Clin Neurophysiol 1994; 91(2):118–30.

Rapoport SI. Functional brain imaging to identify affected subjects genetically at risk for Alzheimer's disease. Proc Natl Acad Sci USA 2000;97(11):5696–8.

Stam CJ, van der Made Y, Pijnenburg YA, Scheltens P. EEG synchronization in mild cognitive impairment and Alzheimer's disease. Acta Neurol Scand 2003;108(2):90–6.

Szupiluk R, Cichocki A. Blind signal separation using second order statistics. Proceedings of SPETO; 2001, p. 485–8.

Tang AC, Pearlmutter BA, Malaszenko NA, Phung DB. Independent components of magnetoencephalography: single-trial response onset time estimation. NeuroImage 2002;17:1773–89.

Tong L, Soon V, Huang YF, Liu R. Indeterminacy and identifiability of blind identification. IEEE Trans CAS 1991;38:499–509.

Tong L, Inouye Y, Liu R. Waveform-preserving blind estimation of multiple independent sources. IEEE Trans Signal Process 1993;41(7): 2461–70.

Vorobyov S, Cichocki A. Blind noise reduction for multisensory signals using ICA and subspace filtering, with application to EEG analysis. Biol Cybern 2002;86(4):293–303.

Wada Y, Nanbu Y, Koshino Y, Yamaguchi N, Hashimoto T. Reduced interhemispheric EEG coherence in Alzheimer disease: analysis during rest and photic stimulation. Alzheimer Dis Assoc Disord 1998;12(3): 175–81.

Wagner AD. Early detection of Alzheimer's disease: an fMRI marker for people at risk. Nat Neurosci 2000;3(10):973–4.

Wechsler D. Wechsler memory scale: revised manual. San Antonio, TX: Psychological Corp.; 1987.

Xu N, Gao X, Hong B, Miao X, Gao S, Yang F. BCI Competition 2003—Data set IIb: enhancing P300 wave detection using ICA-based subspace projections for BCI applications. IEEE Trans Biomed Eng 2004;51(6): 1067–72.

Available online at www.sciencedirect.com
SCIENCE DIRECT®
Neuroscience Letters 379 (2005) 149–151
Neuroscience Letters
www.elsevier.com/locate/neulet

Association study of the chemokine, CXC motif, ligand 1 (CXCL1) gene with sporadic Alzheimer's disease in a Japanese population

Yoshiko Tamura[a,1], Yuji Sakasegawa[a,1], Kazuya Omi[a,b], Hitaru Kishida[a,c], Takashi Asada[d], Hideo Kimura[a], Katsushi Tokunaga[b], Naomi S. Hachiya[a], Kiyotoshi Kaneko[a], Hirohiko Hohjoh[a,*]

[a] *National Center of Neurology and Psychiatry, National Institute of Neuroscience, 4-1-1 Ogawahigashi, Kodaira, Tokyo 187-8502, Japan*
[b] *Department of Human Genetics, Graduate School of Medicine, The University of Tokyo, 7-3-1 Hongo, Bunkyo-ku, Tokyo 113-0033, Japan*
[c] *Department of Neurology, Yokohama City University School of Medicine, Yokohama 236-0004, Japan*
[d] *Department of Neuropsychiatry, Institute of Clinical Medicine, University of Tsukuba, Tsukuba 305-8577, Japan*

Received 25 November 2004; received in revised form 21 December 2004; accepted 22 December 2004

Abstract

Inflammation is profoundly involved in the development of Alzheimer's disease (AD) and other neurodegenerative diseases. Chemokine, CXC motif, ligand 1 (CXCL1; or GRO1) is an inflammatory cytokine and appears to be implicated in the pathogenesis of AD. It is of interest and importance to see if the *CXCL1* gene, mapped on chromosome 4q12–q13, has potential for conferring the predisposition to AD. Here we report on an association study of the *CXCL1* gene with sporadic AD patients in a Japanese population; three single nucleotide polymorphisms (SNPs) in the *CXCL1* locus were investigated in 103 AD patients and 130 healthy individuals. The results indicate that neither genotype frequencies nor allele frequencies of the examined SNPs attained statistical significance even after being stratified by the presence or absence of the *Apolipoprotein E* ε4 allele. Therefore, the data presented here suggests that the *CXCL1* gene could not be associated with the susceptibility to AD in a Japanese population.

Keywords: Alzheimer' disease; Chemokine; CXC motif, ligand 1 (CXCL1); Single nucleotide polymorphisms (SNPs); Association study

Alzheimer's disease (AD) is a progressive neurodegenerative disorder of the elderly, and characterized by accumulation of neurofibrillary tangles and amyloid deposition resulting in the formation of senile plaques in the brain. Sporadic AD other than familial AD appears to be a multifactorial disorder in which both genetic and environmental factors are involved [2]. A genetic factor strongly associated with sporadic AD has been found in the *Apolipoprotein E* (*APOE*) gene: the *APOE ε4* allele increases the predisposition to AD [10,12,13]. It is likely that other genetic factors besides *APOE ε4* could participate in developing AD, and it is of importance and necessary to determine such genetic factors conferring the predisposition to AD.

Chemokines are inflammatory cytokines which have multiple functions in the immune system, and also have effects on cells of the central nervous system [1,3,4,7–9,15–17]. It appears that inflammation is implicated in the pathogeneses of various neurodegenerative disorders including AD [9,14–17]. Previous study suggested that chemokine, CXC motif, ligand 1 (CXCL1; or GRO1) could work as a potent trigger for the ERK1/2 and PI-3 kinase pathway and induce hypermethylation of the tau protein in mouse primary cortical neurons, and also that the immunoreactivity for CXCL1 increased in a subpopulation of neurons in some AD brains [14]. It was further suggested that a chemokine receptor for CXCL1, CXCR2, was expressed on neurons and was strongly upregulated in a subpopulation of senile plaques in AD [9,15].

* Corresponding author. Tel.: +81 42 342 2711x5176; fax: +81 42 346 1748.
E-mail address: hohjohh@ncnp.go.jp (H. Hohjoh).
[1] These authors contributed equally to this work.

0304-3940/$ – see front matter © 2005 Elsevier Ireland Ltd. All rights reserved.
doi:10.1016/j.neulet.2004.12.056

Table 1
Genotype and allele frequencies of the SNPs in the *CXCL1* locus

SNP name (position[a])		Patients (n = 103)	Controls (n = 130)	P	OR (95% CI)
rs3117602	Genotype frequency				
(75,199,137)	C/C	90 (87.4%)	107 (82.3%)	0.43	1.0
	C/A	13 (12.6%)	22 (16.9%)		0.7 (0.3–1.5)
	A/A	0 (0%)	1 (0.8%)		–
	Allele frequency				
	C allele	93.7%	90.7%	0.25	
	A allele	6.3%	9.3%		
rs4074	Genotype frequency				
(75,202,395)	G/G	26 (25.2%)	31 (23.8%)	0.95	1.0
	G/A	55 (53.4%)	72 (55.4%)		0.9 (0.45–1.7)
	A/A	22 (21.4%)	27 (20.8%)		1.0 (0.4–2.0)
	Allele frequency				
	G allele	51.9%	51.6%	0.93	
	A allele	48.1%	48.4%		
rs1429638	Genotype frequency				
(75,204,181)	C/C	46 (44.7%)	59 (45.4%)	0.92	1.0
	C/A	51 (49.5%)	65 (50.0%)		1.0 (0.6–1.7)
	A/A	6 (5.8%)	6 (4.6%)		1.3 (0.4–4.2)
	Allele frequency				
	C allele	69.4%	70.2%	0.82	
	A allele	30.6%	29.8%		

[a] The nucleotide positions are based on the numbering used in the NCBI public location.

These observations lead to the possibility that the *CXCL1* gene could confer the predisposition to sporadic AD, i.e., it may be a genetic risk factor for AD, and stimulate our interest in studying if there is any association between the *CXCL1* gene and AD.

In this study, we investigated three single nucleotide polymorphisms (SNPs) around the *CXCL1* locus mapped on 4q12–q13 in sporadic AD patients and healthy individuals. The subjects were all Japanese: 103 patients with AD (47 men and 56 women; mean age of onset, 70.7 years old) were diagnosed by meeting the National Institute of Neurological and communicative Disorders and Stroke and The Alzheimer's Disease and Related Dementias Association criteria (NINCDS-ADRDA) [11], and 130 unrelated healthy individuals (57 men and 73 women; mean age, 70.9 years old) were examined as controls. Peripheral blood samples were obtained and subjected to isolation of genomic DNA with standard protocols. For a high-throughput analysis, allelic discrimination assay with commercially available Assays-on-Demand SNP Genotyping products (Applied Biosystems) was carried out in 25 μl of 1 × TaqMan Universal PCR Master Mix (Applied Biosystems) containing ~10 ng of genomic DNA and 1.25 μl of an Assays-on-Demand SNP Genotyping product (Applied Biosystems) by using the Applied Biosystems 7300 Real Time PCR System (Applied Biosystems) according the manufacture's instructions. The Assays-on-Demand SNP Genotyping products used (the Assay ID numbers; public ID numbers) were as follows: C_9761059_10; rs3117602 (intergenic SNP), C_11820472_1; rs4074 (intron3 SNP), C_2042711_10; rs1429638 (intergenic SNP). The SNPs cover the *CXCL1* gene and the physical distances between rs3117602 and rs4074 SNPs and between rs4074 and rs1429638 SNPs are approximately 3.3 and 1.8 kb long, respectively. After SNP typing, statistical analyses of the data were carried out using SNPAlyse (DYNACOM, Yokohama, Japan). The presence of Hardy-Weinberg equilibrium was examined by χ^2-test for goodness of fit. Allele distributions between the patients and controls were examined by χ^2-test for independence. As for haplotype analysis, haplotype frequencies and linkage disequilibrium parameters were estimated on the basis of an expectation-maximization algorithm [5]. Case–control haplotype analyses were carried out by using the permutation method to obtain the empirical significance [6]. Each haplotype was tested for association by grouping all other haplotypes together and applying χ^2-test with 1 d.f. P values were estimated on the basis of 10,000 replications.

Table 1 shows the results of the SNP typing in the AD patients and healthy controls. The SNPs examined in this study revealed no significant differences in their genotype frequencies, allele frequencies and allele carrier frequencies between the patients and healthy controls. In addition, none of the polymorphisms in each group deviated from expectations based on Hardy-Weinberg equilibrium at a significance level of 0.01. Accordingly, although there was a limitation in the number of the subjects used in this study, i.e., the numbers of the patients and controls used were small; the typing data suggested that the *CXCL1* gene could not be a major risk factor conferring the susceptibility to AD at least. We further examined allelic associations (haplotypes) among the rs3117602, rs4074 and rs1429638 SNPs. As a result, strong

Table 2
Estimated haplotypes and their frequencies

Haplotypes[a]	Patients ($n=103$), HF (%)	Controls ($n=130$), HF (%)	P
C–G–C	51.9	50.5	0.75
C–A–A	29.4	28.9	0.66
C–A–C	12.3	11.4	0.75
A–A–C	5.2	7.5	0.32

HF: haplotype frequency.
[a] Estimated haplotypes with the rs3117602, rs4074 and rs1429638 SNPs are indicated and the haplotypes with 5% or more of their frequencies are shown.

allelic associations (haplotypes) among the SNPs were detectable in either the healthy controls or AD patients (Table 2); but, the estimated haplotype frequencies resulted in no significant difference between the patients and controls. We must add that further analyses stratified by either the presence or absence of the *APOE ε4* allele resulted in no statistical significance, although the difference in the frequency of the *APOE ε4* allele alone between the patients and controls attained statistical significance ($P=0.0079$). Taking all the data together, it is suggested that the *CXCL1* gene is not associated with the susceptibility to sporadic AD. Since inflammation appears to be implicated in the development of AD, it is conceivable that the *CXCL1* gene could contribute to only inflammatory response in the course of the development of AD, but not participate in the pathogenesis of AD as a genetic factor conferring the predisposition to AD.

Acknowledgments

We would like to thank Dr. N. Minami for providing the DNA samples of patients. This work was supported by the Millennium Project of Alzheimer's Disease in Japan.

References

[1] A. Bajetto, R. Bonavia, S. Barbero, T. Florio, G. Schettini, Chemokines and their receptors in the central nervous system, Front Neuroendocrinol. 22 (2001) 147–184.
[2] D. Blacker, L. Bertram, A.J. Saunders, T.J. Moscarillo, M.S. Albert, H. Wiener, R.T. Perry, J.S. Collins, L.E. Harrell, R.C. Go, A. Mahoney, T. Beaty, M.D. Fallin, D. Avramopoulos, G.A. Chase, M.F. Folstein, M.G. McInnis, S.S. Bassett, K.J. Doheny, E.W. Pugh, R.E. Tanzi, Results of a high-resolution genome screen of 437 Alzheimer's disease families, Hum. Mol. Genet. 12 (2003) 23–32.
[3] R. Bonavia, A. Bajetto, S. Barbero, P. Pirani, T. Florio, G. Schettini, Chemokines and their receptors in the CNS: expression of CXCL12/SDF-1 and CXCR4 and their role in astrocyte proliferation, Toxicol. Lett. 139 (2003) 181–189.
[4] C.M. Coughlan, C.M. McManus, M. Sharron, Z. Gao, D. Murphy, S. Jaffer, W. Choe, W. Chen, J. Hesselgesser, H. Gaylord, A. Kalyuzhny, V.M. Lee, B. Wolf, R.W. Doms, D.L. Kolson, Expression of multiple functional chemokine receptors and monocyte chemoattractant protein-1 in human neurons, Neuroscience 97 (2000) 591–600.
[5] L. Excoffier, M. Slatkin, Maximum-likelihood estimation of molecular haplotype frequencies in a diploid population, Mol. Biol. Evol. 12 (1995) 921–927.
[6] D. Fallin, A. Cohen, L. Essioux, I. Chumakov, M. Blumenfeld, D. Cohen, N.J. Schork, Genetic analysis of case/control data using estimated haplotype frequencies: application to APOE locus variation and Alzheimer's disease, Genome Res. 11 (2001) 143–151.
[7] J.K. Harrison, C.M. Barber, K.R. Lynch, cDNA cloning of a G-protein-coupled receptor expressed in rat spinal cord and brain related to chemokine receptors, Neurosci. Lett. 169 (1994) 85–89.
[8] J.K. Harrison, Y. Jiang, S. Chen, Y. Xia, D. Maciejewski, R.K. McNamara, W.J. Streit, M.N. Salafranca, S. Adhikari, D.A. Thompson, P. Botti, K.B. Bacon, L. Feng, Role for neuronally derived fractalkine in mediating interactions between neurons and CX3CR1-expressing microglia, Proc. Natl. Acad. Sci. U.S.A. 95 (1998) 10896–10901.
[9] R. Horuk, A.W. Martin, Z. Wang, L. Schweitzer, A. Gerassimides, H. Guo, Z. Lu, J. Hesselgesser, H.D. Perez, J. Kim, J. Parker, T.J. Hadley, S.C. Peiper, Expression of chemokine receptors by subsets of neurons in the central nervous system, J. Immunol. 158 (1997) 2882–2890.
[10] S.M. Laws, E. Hone, S. Gandy, R.N. Martins, Expanding the association between the APOE gene and the risk of Alzheimer's disease: possible roles for APOE promoter polymorphisms and alterations in APOE transcription, J. Neurochem. 84 (2003) 1215–1236.
[11] G. McKhann, D. Drachman, M. Folstein, R. Katzman, D. Price, E.M. Stadlan, Clinical diagnosis of Alzheimer's disease: report of the NINCDS-ADRDA Work Group under the auspices of Department of Health and Human Services Task Force on Alzheimer's Disease, Neurology 34 (1984) 939–944.
[12] M. Michikawa, K. Yanagisawa, Apolipoprotein E4 induces neuronal cell death under conditions of suppressed de novo cholesterol synthesis, J. Neurosci. Res. 54 (1998) 58–67.
[13] A.M. Saunders, W.J. Strittmatter, D. Schmechel, P.H. George-Hyslop, M.A. Pericak-Vance, S.H. Joo, B.L. Rosi, J.F. Gusella, D.R. Crapper-MacLachlan, M.J. Alberts, et al., Association of apolipoprotein E allele epsilon 4 with late-onset familial and sporadic Alzheimer's disease, Neurology 43 (1993) 1467–1472.
[14] M. Xia, B.T. Hyman, GROalpha/KC a chemokine receptor CXCR2 ligand, can be a potent trigger for neuronal ERK1/2 and PI-3 kinase pathways and for tau hyperphosphorylation—a role in Alzheimer's disease? J. Neuroimmunol. 122 (2002) 55–64.
[15] M. Xia, S. Qin, M. McNamara, C. Mackay, B.T. Hyman, Interleukin-8 receptor B immunoreactivity in brain and neuritic plaques of Alzheimer's disease, Am. J. Pathol. 150 (1997) 1267–1274.
[16] M.Q. Xia, B.J. Bacskai, R.B. Knowles, S.X. Qin, B.T. Hyman, Expression of the chemokine receptor CXCR3 on neurons and the elevated expression of its ligand IP-10 in reactive astrocytes: in vitro ERK1/2 activation and role in Alzheimer's disease, J. Neuroimmunol. 108 (2000) 227–235.
[17] M.Q. Xia, B.T. Hyman, Chemokines/chemokine receptors in the central nervous system and Alzheimer's disease, J. Neurovirol. 5 (1999) 32–41.

Available online at www.sciencedirect.com
SCIENCE DIRECT®
Neuroscience Letters 382 (2005) 269–274
Neuroscience Letters
www.elsevier.com/locate/neulet

Voxel-based morphometry to discriminate early Alzheimer's disease from controls

Yoko Hirata[a,d], Hiroshi Matsuda[a,b,*], Kiyotaka Nemoto[a,c], Takashi Ohnishi[a], Kentaro Hirao[a], Fumio Yamashita[c], Takashi Asada[c], Satoshi Iwabuchi[d], Hirotsugu Samejima[d]

[a] *Department of Radiology, National Center Hospital for Mental, Nervous and Muscular Disorders, National Center of Neurology and Psychiatry, 4-1-1 Ogawahigashi, Kodaira, Tokyo 187-8551, Japan*
[b] *Department of Nuclear Medicine, Saitama Medical School, 38 Morohongo, Moroyama-machi, Iruma-gun, Saitama 350-0495, Japan*
[c] *Department of Neuropsychiatry, Institute of Clinical Medicine, University of Tsukuba, 1-1-1 Tennoudai, Tsukuba, Ibaraki, 305-0006, Japan*
[d] *Department of Neurosurgery, Toho Ohashi Hospital, 2-17-6 Ohashi, Meguro, Tokyo 153-8515, Japan*

Received 23 December 2004; received in revised form 18 February 2005; accepted 13 March 2005

Abstract

We assessed the accuracy of voxel-based morphometry (VBM) using a three-dimensional T1-weighted MRI in discriminating Alzheimer's disease (AD) in the very early stage of amnestic type of mild cognitive impairment and age-matched healthy controls. We randomly divided these subjects into two groups. The first group comprising 30 AD patients and 41 controls was used to identify the area with the most significant gray matter loss in patients compared to normal controls based on the voxel-based analysis of a group comparison. The second group comprising 31 patients and 41 controls was used to determine the discrimination accuracy of VBM. A Z-score map for a gray matter image of a subject was obtained by comparison with mean and standard deviation gray matter images of the controls for each voxel after anatomical standardization and voxel normalization to global mean using the following equation; Z-score = ([control mean] − [individual value])/(control S.D.). Receiver operating characteristic curves for a Z-score in the bilateral medial temporal areas including the entorhinal cortex with the most significant loss in the first group showed a high discrimination accuracy of 87.8%. This result would open up a possibility for early diagnosis of AD using VBM.

Keywords: MRI; Alzheimer's disease; Voxel-based morphometry; Mild cognitive impairment

The fact that recently available medications like cholinesterase inhibitors delay the progression of Alzheimer's disease (AD) has increased the urgency of diagnosing AD at an early stage. Numerous structural MRI studies have demonstrated that atrophy of the medial temporal lobe, including the hippocampus and entorhinal cortex, is a sensitive marker of early AD [6,15]. Moreover it has been suggested that atrophy of medial temporal lobe structures might predict progression from mild cognitive impairment (MCI) to AD [16,25]. Of medial temporal lobe structures, it has been argued that decreased entorhinal cortex volume might be a particularly sensitive predictor of AD on the basis of tangle deposition of early entorhinal cortex involvement in AD with subsequent spread to the hippocampus proper [3]. Killiany et al. [16] used MRI to measure the volumes of the entorhinal cortex and hippocampus in 137 individuals, and found that the volume of the entorhinal cortex distinguished the subjects who were destined to develop dementia with considerable accuracy, whereas the hippocampus measure did not.

However, it is difficult to evaluate atrophy of the entorhinal cortex by visual inspection. On the other hand, volumetric

* Corresponding author. Tel.: +81 49 276 1302; fax: +81 49 276 1301.
E-mail address: matsudah@saitama-med.ac.jp (H. Matsuda).

0304-3940/$ – see front matter © 2005 Elsevier Ireland Ltd. All rights reserved.
doi:10.1016/j.neulet.2005.03.038

assessment of the entorhinal cortex in routine clinical practice requires the very time-consuming nature of region of interest analysis, which is dependent on the expertise of the tracers and lacks an automated volume measurement technique. Recently a new automated method of measuring brain atrophy has been developed [2,21]. This new method of voxel-based morphometry (VBM) objectively maps gray matter loss on a voxel-by-voxel basis after anatomical standardization analogous to that used in functional neuroimaging. The advantage of VBM over analyses based on region of interest is that VBM produces an unbiased result from exploration of the whole brain. This approach has been reported to show higher accuracy of discriminating AD and controls than region of interest-based analysis [24]. The present VBM study was undertaken to evaluate the ability to discriminate very early AD patients from age-matched controls using a newly developed software program.

We retrospectively chose 61 patients (32 men and 29 women) with a clinical diagnosis of probable AD patients according to the National Institute of Neurological and Communicative Disorders and Stroke and the Alzheimer's Disease and Related Disorders Association criteria (NINCDS-ADRDA) [18]. At the initial visit, they showed verbal and/or visual episodic memory impairment in delayed recall, as defined by performance 1.5S.D. below the mean for age-matched normal controls in learning of a list of 10 words, 15-item story recall test, and Rey–Osterrieth complex figure test [12]. They had no apparent loss in general cognitive, behavioral, or functional status and corresponded to the criteria of amnestic type of MCI proposed by Petersen et al. [22] or 0.5 in Clinical Dementia Rating [13]. They ranged in age from 48 to 87 years with a mean ± S.D. of 70.6 ± 8.4. The Mini-Mental State Examination (MMSE) [8] score ranged from 24 to 29; 26.0 ± 1.5 at the initial visit. During the subsequent follow-up period of two to six years, the subjects showed progressive cognitive decline and eventually fulfilled the diagnosis of probable AD according to the NINCDS-ADRDA.

Eighty-two control subjects (39 men and 43 women, age; 54–86 years, mean 70.1, S.D. 7.7) were healthy volunteers with no memory impairment or cognitive disorders. Their performance was within normal limits both on the Wechsler Memory Scale—Revised and Wechsler Adult Intelligence Scale—Revised. The MMSE score ranged from 26 to 30; 28.7 ± 1.5. They did not differ significantly in age or education from the AD patients. The Ethics Committee of the National Center of Neurology and Psychiatry approved this study for healthy volunteers, all of whom provided informed consent to participate.

All of the subjects were right handed and screened by questionnaire and medical history to exclude those with medical conditions potentially affecting the central nervous system. In addition, none of them had asymptomatic cerebral infarction detected by T2-weighted MRI.

All MRI studies were performed on a 1.0-T system (Magnetom Impact Expert, Siemens, Erlangen, Germany). A three-dimensional volumetric acquisition of a T1-weighted gradient echo sequence produced a gapless series of thin sagittal sections using an MPRage sequence (echo time/repetition time, 4.4/11.4; flip angle, 15°; acquisition matrix, 256 × 256; 1 excitation; field of view, 31.5 cm; slice thickness, 1.23 mm).

The VBM for an MR image was performed as described in our previous study [17] based on the method proposed by Baron et al. [2]. The theory and algorithm of this VBM were well-documented by Ashburner and Friston [1]. The acquired MR images were reformatted to gapless 2-mm-thick transaxial images. Images were analyzed using Statistical Parametric Mapping 2002 (SPM2) (Wellcome Department of Imaging Neuroscience, London, UK) running on MATLAB (The MathWorks, Inc., Sherborn, MA, USA). Anatomical standardization fitted each individual brain to a standard template brain (Talairach and Tournoux [23]) in three-dimensional space, so as to correct for differences in brain size and shape and facilitate intersubject averaging. In the first anatomical standardization, only 12-parameter affine transformation was used. Normalized MR images were then segmented into gray matter, white matter, cerebrospinal fluid, and other compartments using a modified version of the clustering algorithm, the maximum likelihood "mixture model" algorithm. The segmentation procedure involves calculating for each voxel a Bayesian probability of belonging to each tissue class based on a priori MRI information with a non-uniformity correction. The segmented gray matter images were then subjected to an affine and non-linear anatomical standardization using a template of a priori gray matter. The anatomically standardized gray matter images were smoothed with an isotropic Gaussian kernel 12 mm in full width at half maximum (FWHM) to use the partial volume effect to create a spectrum of gray matter intensities. The gray matter intensities are equivalent to the weighted average of gray matter voxels located in the volume fixed by the smoothing kernel. Regional intensities can therefore be taken as equivalent to gray matter concentration [1].

We randomly selected 30 patients and 41 healthy volunteers as the first group to establish the region with the most significant decline of gray matter concentrations in patients using SPM2. The patients and healthy volunteers were compared using the "compare-population one scan/subject" routine in SPM2. The "proportional scaling" routine was used to control for individual variation in global mean intensities. The resulting set of values for each contrast constituted a statistical parametric map of the t-statistic SPM$\{t\}$. The SPM$\{t\}$ were transformed to the unit normal distribution {SPM(Z)} and thresholded at $P < 0.001$. The significance of each region was estimated with a threshold of $P = 0.01$ with correction for multiple non-independent comparisons. Extent threshold was set to 0 voxels.

A software program running on Windows XP for analysis of gray matter images was newly developed to discriminate between the remaining 31 patients and 41 healthy volunteers as the second group. Each gray matter image of the patients was compared to the mean and S.D. of gray matter images

of the 41 healthy volunteers using voxel-by-voxel Z-score analysis after voxel normalization to global mean intensities; Z-score = ([control mean] − [individual value])/(control S.D.) as previously reported by Minoshima et al. in a PET study [20]. These Z-score maps were displayed by overlay on tomographic sections. We designated this software program as the voxel-based specific region analysis for Alzheimer's disease (VSRAD) which can automatically analyze three-dimensional T1-weighted MRI data as a series of segmentation, anatomical standardization and smoothing using SPM2 without a Matlab program, and Z-score analysis. This program registered the SPM{t} results for significant decline of gray matter concentrations in patients determined by group comparison in the first group as a specific region of interest.

Each gray matter image of one of the 41 healthy volunteers was also compared with the averaged gray matter image of the remaining 40 healthy volunteers in the same manner as in the patients. Using the averaged value of positive Z-scores in the specific region of interest in a Z-score map as the threshold, receiver operating characteristic (ROC) curves were determined using the ROCKIT 0.9β and the PlotROC programs developed by Metz et al. (http://xray.bsd.uchicago.edu/krl) [19]. The program calculates the area under the ROC curves (Az), accuracy, sensitivity and specificity. Accuracy was determined as the value at the point where the sensitivity is the same as the specificity on the ROC curve.

The SPM2 analysis demonstrated significant declines of gray matter concentrations of patients only in the left (−17, −8, −18, x, y, z; $Z = 5.47$) and the right (16, −9, −18, x, y, z; $Z = 5.42$) parahippocampal gyri in the first group (Fig. 1). These regions correspond to Brodmann areas 28 (entorhinal area) and 34 (dorsal entorhinal area) and constitute the entire entorhinal area together [4]. These regions of bilateral parahippocampal areas are delineated as specific regions of interest for very early AD.

Then the averaged value of positive Z-scores in these bilateral specific regions of interest was obtained in a Z-score map (Fig. 2) in the second group using a VSRAD software program. Using these averaged Z-score values in these specific regions of interest the ROC curves for discrimination of patients from healthy volunteers were computed (Fig. 3). The Az and accuracy were 0.949 (95% confidence interval 0.880–0.982) and 87.8%, respectively.

In the present study, automated voxel-based analysis using a Z-score value in the bilateral medial temporal areas including the entorhinal cortex after anatomical standardization of gray matter images revealed a high accuracy of 87.8% in the discrimination of AD patients in the very early stage

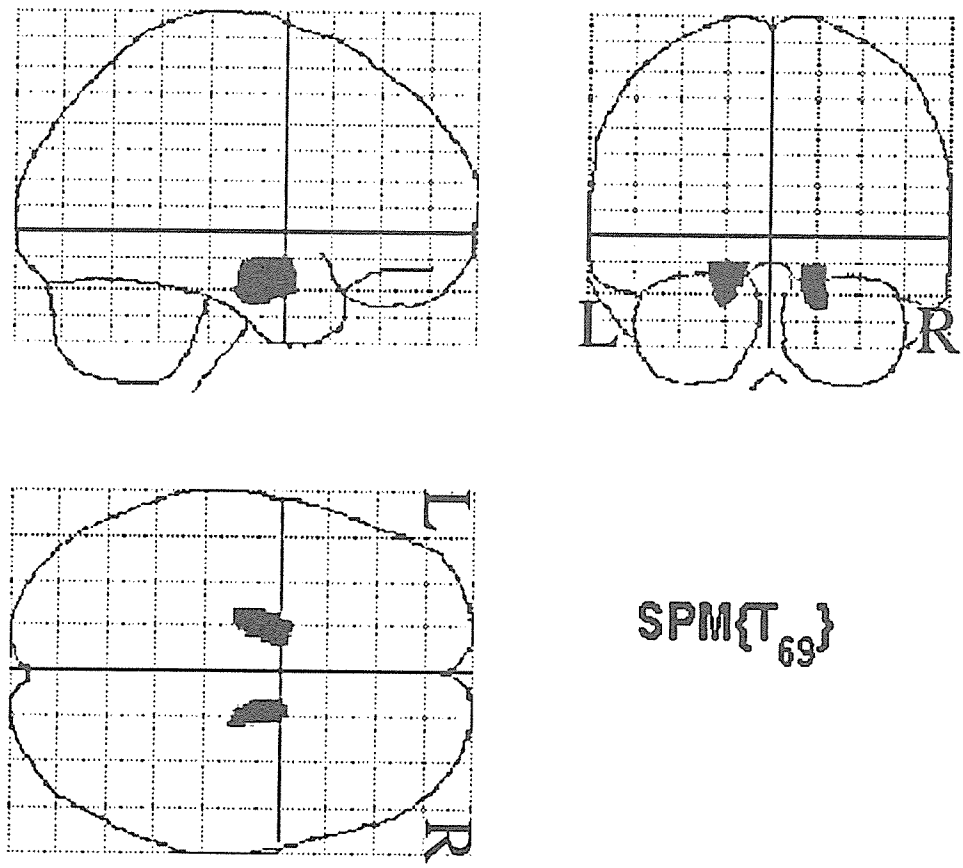

Fig. 1. Maximum intensity projections of SPM2 results for significant decline of gray matter concentration in very early AD patients as compared with age-matched healthy volunteers (−17, −8, −18, x,y,z; $Z = 5.47$; 16, −9, −18, x,y,z; $Z = 5.42$). These regions correspond to bilateral Brodmann areas 28 and 34. Height threshold <0.001, corrected for multiple comparisons.

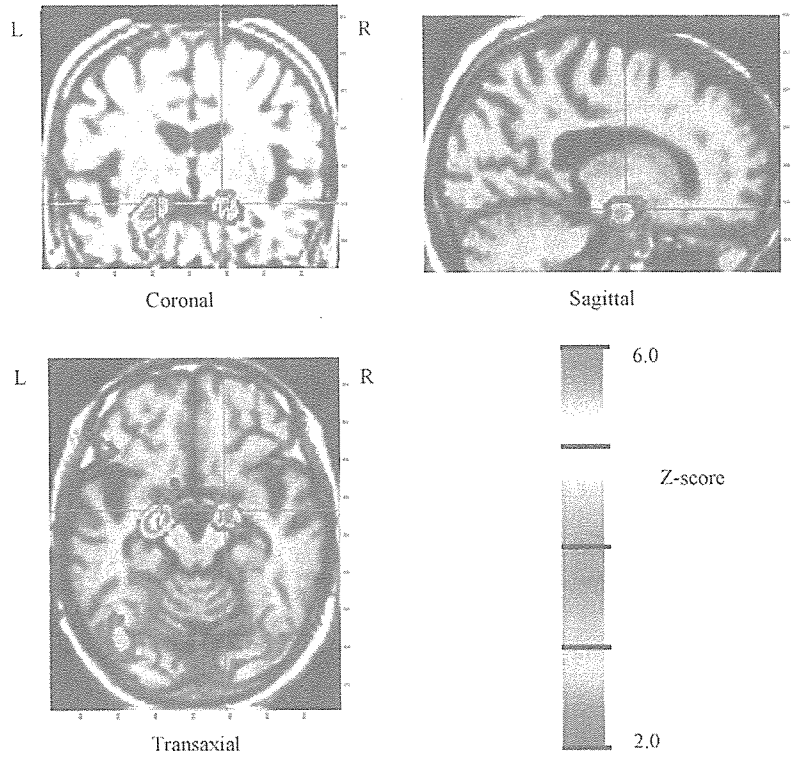

Fig. 2. Automated voxel-by-voxel Z-score analysis by comparison of a gray matter image for an 82-year-old woman at the stage of MCI before conversion to AD with MMSE of 24 with the mean and standard deviation gray matter images of healthy volunteers after normalization to global mean voxel intensities. The color-scaled Z-score maps ranging from 2.0 to 6.0 were displayed by overlaying on orthogonal sections of the anatomically standardized MRI of the patient. Red lines enclose areas with the most significant decline of gray matter concentration in very early AD obtained from group comparison with healthy volunteers by SPM2. The averaged value of positive Z-scores in this specific region is 2.4.

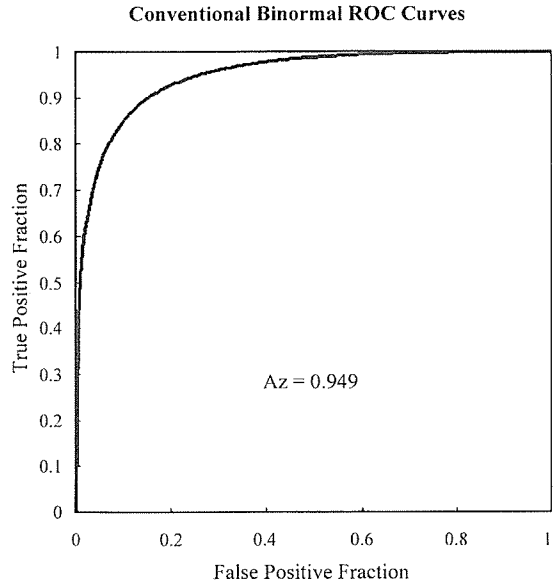

Fig. 3. Receiver operating characteristic (ROC) curves for discrimination between probable AD patients at the very early stage of amnestic MCI and healthy volunteers when thresholding at the averaged values of positive Z-scores in the medial temporal areas including the entorhinal cortex. The Az and accuracy were 0.949 and 87.8%, respectively.

from healthy volunteers. We adopted the VBM procedure proposed by Baron et al. [2] in which segmentation of the MR images based on an affine only and reversible normalization was followed by the full spatial normalization process with both affine transform and non-linear warping only onto the segmented gray matter set based on the standard gray matter template. Presumably because of segmentation errors due to partial volume effects inherently created by warping, the use of standard full normalization prior to segmentation appears to increase the risk of misclassification of non-brain tissue as gray matter voxels.

Neuropathological studies have provided detailed information about which specific brain regions are selectively affected in the earliest stage of AD. The initial neuronal lesions of the neurofibrillary tangles and neuritic plaques appear to occur in the entorhinal cortex, a portion of the anterior parahippocampal gyrus that receives projections from widespread limbic and association areas and gives rise to the perforant pathway, the major cortical excitatory input to the hippocampus itself [10,14]. Some layers of the entorhinal cortex undergo 40–60% neuronal depopulation even in the earliest phase of AD, when memory impairments and patient complaints are subtle and the symptoms do not reach the threshold for a diagnosis of AD [10]. In the present VBM study, SPM2 revealed gray matter loss selectively in the bilateral medial

temporal areas including entorhinal areas in very early AD in good agreement with these pathological changes in the amnestic stage of AD. Frisoni et al. [9] reported the most significant gray matter loss in bilateral hippocampal/amygdalar complex using SPM99 in three very early AD patients with MMSE scores of over 24. Using SPM99, Chetelat et al. [5] also reported significant gray matter loss predominantly affecting the hippocampal region and cingulate gyri in patients with amnestic MCI.

A method for automated diagnosis of gray matter loss was developed in the present study. In this software program, voxel-based analysis was performed using a Z-score map calculated from comparison of a patient's data with the control database. This program has the advantage of being able to incorporate SPM2 results into automated analysis of Z-score values as a specific region of interest. The specific region of interest can be determined by group comparison of gray matter images for patients with a neuropsychiatric disease with those for healthy volunteers using SPM2. Herholtz et al. [11] developed a similar original software program based on an automated voxel-based procedure after anatomical image standardization for discrimination between probable AD and controls using ^{18}F-fluorodeoxyglucose PET. They reported 84% sensitivity and 93% specificity for discrimination between very mild probable AD with MMSE over 24 and controls. The current VBM study on very mild probable AD provided almost the same accuracy as that in a PET study.

Finally we must refer to several study limitations. First, the sample size is too small to conclude whether this VBM approach to early diagnosis of AD is truly useful for a routine clinical MRI study or not. If this approach is extended to a multi-center study for a larger sample size, we have to resolve the systematic variations in raw original structural images obtained from different MR scanners. Second, we investigated amnestic MCI patients who all converted to AD. The outcome for any patient with MCI is uncertain because many subjects may remain stable or ever revert to a normal state, while others progress to dementia. Accordingly the predictive study using this VBM approach is much more important for MCI conversion to AD. Third, although the present cross-sectional study provided high discrimination accuracy between AD and controls, it has been reported that longitudinal measures of the annual atrophy rate of the entorhinal cortex elevated the discrimination accuracy of early AD and controls from 77% for the cross-sectional baseline study to 82% [7]. This fully automated software with incorporation of a specific region for longitudinal changes in very early AD would be expected to enhance the discrimination accuracy of VBM in follow-up studies. Fourth, VBM does not have the anatomical precision attainable by classic ROI-based volumetric studies. This is because of the need to anatomically standardize and smooth the data in order to reduce the effect of intersubject differences in normal gyral anatomy and in turn to allow for a statistical, voxelwise analysis across subjects. However, this limitation should not detract from the considerable advantages of the voxel-based analysis in terms of efficiency, comprehensiveness, and freedom from observer bias.

In conclusion, an automated analysis of VBM using a Z-score map was applied to discrimination between probable AD patients at the very early stage of amnestic MCI and age-matched healthy volunteers. ROC analysis of the averaged value of positive Z-scores in the bilateral medial temporal areas including the entorhinal cortex for the very early stage of probable AD determined by SPM2 demonstrated discrimination accuracy of 87.8%. The VBM would thus lead to the possibility for the early diagnosis of AD in an MRI study.

Acknowledgments

We are very thankful to the technical staff in our hospital for data acquisition of MRI, and Mr. John Gelblum for his proofreading of this manuscript.

References

[1] J. Ashburner, K.J. Friston, Voxel-based morphometry—the methods, Neuroimage 11 (2000) 805–821.
[2] J.C. Baron, G. Chetelat, B. Desgranges, G. Perchey, B. Landeau, V. De. La. Sayette, F. Eustache, In vivo mapping of gray matter loss with voxel-based morphometry in mild Alzheimer's disease, Neuroimage 14 (2001) 298–309.
[3] H. Braak, E. Braak, Evolution of the neuropathology of Alzheimer's disease, Acta Neurol. Scand. Suppl. 165 (1996) 3–12.
[4] K. Brodmann, Vergleichende Lokalisationslehre der Groshirnrinde, Barth, Leipzig, 1925.
[5] G. Chetelat, B. Desgranges, V. De. La. Sayette, F. Viader, F. Eustache, J.C. Baron, Mapping gray matter loss with voxel-based morphometry in mild cognitive impairment, NeuroReport 13 (2002) 1939–1943.
[6] A.T. Du, N. Schuff, D. Amend, M.P. Laakso, Y.Y. Hsu, W.J. Jagust, B.L. Miller, B.R. Reed, D. Mungas, K. Yaffe, H.C. Chui, M.W. Weiner, Magnetic resonance imaging of the entorhinal cortex and hippocampus in mild cognitive impairment and Alzheimer's disease, J. Neurol. Neurosurg. Psychiatry 71 (2001) 441–447.
[7] A.T. Du, N. Schuff, X.P. Zhu, W.J. Jagust, B.L. Miller, B.R. Reed, J.H. Kramer, D. Mungas, K. Yaffe, H.C. Chui, M.W. Weiner, Atrophy rates of entorhinal cortex in AD and normal aging, Neurology 60 (2003) 481–486.
[8] M.F. Folstein, S.E. Folstein, P.R. McHugh, Mini-Mental State: a practical method for grading the cognitive state of patients for the clinician, J. Psychiatr. Res. 12 (1975) 189–198.
[9] G.B. Frisoni, C. Testa, A. Zorzan, F. Sabattoli, A. Beltramello, H. Soininen, M.P. Laakso, Detection of grey matter loss in mild Alzheimer's disease with voxel based morphometry, J. Neurol. Neurosurg. Psychitatry 73 (2002) 657–664.
[10] T. Gomez-Isla, J.L. Price, D.W. McKeel Jr., J.C. Morris, J.H. Growdon, B.T. Hyman, Profound loss of layer II entorhinal cortex neurons occurs in very mild Alzheimer's disease, J. Neurosci. 16 (1996) 4491–4500.
[11] K. Herholz, E. Salmon, D. Perani, J.C. Baron, V. Holthoff, L. Frolich, P. Schonknecht, K. Ito, R. Mielke, E. Kalbe, G. Zundorf, X. Delbeuck, O. Pelati, D. Anchisi, F. Fazio, N. Kerrouche, B. Desgranges, F. Eustache, B. Beuthien-Baumann, C. Menzel, J. Schroder, T. Kato, Y. Arahata, M. Henze, W.D. Heiss, Discrimination between Alzheimer dementia and controls by automated analysis of multicenter FDG PET, Neuroimage 17 (2002) 302–316.

[12] J.R. Hodges, Cognitive Assessment for Clinicians, Oxford Medical Publications, Oxford, 1993.
[13] C.P. Hughes, L. Berg, W.L. Danziger, L.A. Coben, R.L. Martin, A new clinical scale for the staging of dementia, Br. J. Psychiatry 140 (1982) 566–572.
[14] B.T. Hyman, G.W. Van Hoesen, C. Kromer, A.R. Damasio, Alzheimer's disease: cell specific pathology isolates the hippocampal formation, Science 225 (1984) 1168–1170.
[15] R.J. Killiany, T. Gomez-Isla, M. Moss, R. Kikinis, T. Sandor, F. Jolesz, R. Tanzi, K. Jones, B.T. Hyman, M.S. Albert, Use of structural magnetic resonance imaging to predict who will get Alzheimer's disease, Ann. Neurol. 47 (2000) 430–439.
[16] R.J. Killiany, B.T. Hyman, T. Gomez-Isla, M.B. Moss, R. Kikinis, F. Jolesz, R. Tanzi, K. Jones, M.S. Albert, MRI measures of entorhinal cortex vs hippocampus in preclinical AD, Neurology 58 (2002) 1188–1196.
[17] H. Matsuda, N. Kitayama, T. Ohnishi, T. Asada, S. Nakano, S. Sakamoto, E. Imabayashi, A. Kato, Longitudinal evaluation of both morphologic and functional changes in the same individuals with Alzheimer's disease, J. Nucl. Med. 43 (2002) 304–311.
[18] G. McKhann, D. Drachman, M. Folstein, R. Katzman, D. Prie, E.M. Stadlan, Clinical diagnosis of Alzheimer's disease: Report of the NINCDS-ADRDA work group under the auspices of department of health and human service task force on Alzheimer's disease, Neurology 34 (1984) 939–944.
[19] C.E. Metz, B.A. Herman, C.A. Roe, Statistical comparison of two ROC-curve estimates obtained from partially-paired datasets, Med. Decis. Making 18 (1998) 110–121.
[20] S. Minoshima, K.A. Frey, R.A. Koeppe, N.L. Foster, D.E. Kuhl, A diagnostic approach in Alzheimer's disease using three-dimensional stereotactic surface projections of fluorine-18-FDG PET, J. Nucl. Med. 36 (1995) 1238–1248.
[21] T. Ohnishi, H. Matsuda, T. Tabira, T. Asada, M. Uno, Changes in brain morphology in Alzheimer disease and normal aging: is Alzheimer disease an exaggerated aging process? Am. J. Neuroradiol. 22 (2001) 1680–1685.
[22] R.C. Petersen, R. Doody, A. Kurz, R.C. Mohs, J.C. Morris, P.V. Rabins, K. Ritchie, M. Rossor, L. Thal, B. Winblad, Current concepts in mild cognitive impairment, Arch. Neurol. 58 (2001) 1985–1992.
[23] J. Talairach, P. Tourmoux, Co-Planar Stereotaxic Atlas of the Human Brain, Tieme Medical, New York, 1988.
[24] C. Testa, M.P. Laakso, F. Sabattoli, R. Rossi, A. Beltramello, H. Soininen, G.B. Frisoni, A comparison between the accuracy of voxel-based morphometry and hippocampal volumetry in Alzheimer's disease, J. Magn. Reson. Imaging 19 (2004) 274–282.
[25] P.J. Visser, F.R. Verhey, P.A. Hofman, P. Scheltens, J. Jolles, Medial temporal lobe atrophy predicts Alzheimer's disease in patients with minor cognitive impairment, J. Neurol. Neurosurg. Psychiatry 72 (2002) 491–497.

Available online at www.sciencedirect.com
SCIENCE DIRECT®
Neuroscience Letters 386 (2005) 111–115
Neuroscience Letters
www.elsevier.com/locate/neulet

Immunohistochemical study of the hnRNP A2 and B1 in the hippocampal formations of brains with Alzheimer's disease

Katsuyoshi Mizukami [a,*,1], Masanori Ishikawa [a], Masahiko Iwakiri [a], Milos D. Ikonomovic [b], Steven T. Dekosky [b], Hiroshi Kamma [c], Takashi Asada [a]

[a] *Department of Psychiatry, Institute of Clinical Medicine, University of Tsukuba, 1-1-1 Tennodai, Tsukuba City, Ibaraki 305-8575, Japan*
[b] *Western Psychiatric Institute and Clinic University of Pittsburgh, 3811 O'Hara Street, Pittsburgh, PA 15213, USA*
[c] *Department of Pathology, Institute of Basic Sciences, University of Tsukuba, 1-1-1 Tennodai, Tsukuba city, Ibaraki 305-8575, Japan*

Received 5 April 2005; received in revised form 18 May 2005; accepted 31 May 2005

Abstract

To elucidate the post-transcriptional regulation in the subjects with Alzheimer's disease (AD), we employed immunohistochemical techniques and examined the expression of the heterogeneous nuclear ribonucleoprotein (hnRNP) A2 and B1 in the hippocampus with neurofibrillary tangle (NFT) neuropathology. In the mildly affected subjects (Braak stages I and II), the most intense A2 immunoreactivity was observed in the CA3 to CA1 neurons. In the moderately (Braak stages III and IV) and severely affected subjects (Braak stages V and VI), the CA1 region demonstrated a decrease in the number of A2 immunoreactive neurons and in immunoreactivity in the remaining neurons, while within the CA4 to CA2 in the severely affected subjects, the majority of neurons showed increased A2 immunoreactivity. An intense B1 immunoreactivity was observed throughout the CA subfields. In the CA1 subfield of the moderately affected subjects and in the extensive hippocampal regions of the severely affected subjects, a decrease in B1 immunoreactivity was observed. Double-immunolabeling studies demonstrated that tangle-bearing neurons reduced A2 and B1 immunoreactivity. Our study suggests that hnRNP A2 and B1 display different responses in the AD hippocampus, and further suggests that the post-transcriptional regulation is disturbed in neurons of the AD hippocampus.

Keywords: Alzheimer's disease; Heterogeneous nuclear ribonucleoprotein (hnRNP); Hippocampus; mRNA; Post-transcriptional regulation

Alzheimer's disease (AD) is characterized pathologically by the presence of amyloid beta protein (Aβ) deposits and neurofibrillary tangles (NFT) and the loss of nerve cells and synapses. It is well-documented that certain regions in the hippocampus are prone to developing AD pathology, whereas other regions display a greater resistance. In exploring the molecular basis underlying the selected vulnerability of neurons in the AD brain, we believe it is important to understand the alterations in the transcriptional and post-transcriptional regulation of neurons. Although a growing body of evidence suggests that some pathological incidents in the AD brain are associated with post-transcriptional regulation [1,7,13,21,22], and overall post-transcriptional regulation is reported to be reduced in severely affected subjects with AD [19], the details of the post-transcriptional regulation in AD brain remains unclear. Heterogeneous nuclear ribonucleoprotein (hnRNP) proteins directly bind to pre-mRNA forming a large multiprotein–RNA complex and have important roles in the post-transcriptional regulations, such as the splicing and transport of mRNAs [4,18]. hnRNP A2 and B1 are produced by alternative splicing from a single copy gene [12], and they are one of the most abundant and important nuclear RNA-binding proteins [4]. The expression of these hnRNP proteins may, in part, reflect post-transcriptional regulation [15]. In this study, to elucidate neuronal post-transcriptional regulations, we

* Corresponding author. Tel.: +81 298 53 3210; fax: +81 298 53 3183.
E-mail address: mizukami@md.tsukuba.ac.jp (K. Mizukami).
[1] Tel.: 81 298 53 3182; fax: 81 298 53 3182.

0304-3940/$ – see front matter © 2005 Elsevier Ireland Ltd. All rights reserved.
doi:10.1016/j.neulet.2005.05.070

employed immunohistochemical techniques to examine the alterations in hnRNP A2 and B1 proteins in the hippocampus from elderly subjects with NFT neuropathology.

Postmortem brain tissue was obtained from 17 elderly subjects (Table 1): 13 with a clinical diagnosis of AD (77.7 ± 12.7 years) and 4 age-matched cognitively normal control subjects (73.3 ± 16.5 years). The mean postmortem interval (PMI) and brain weight of the cases were 6.5 ± 4.9 h and 1167 ± 126 g, respectively. For non-demented subjects, clinical evaluations were largely based on retrospective analysis of medical records and interviews with their physicians and immediate family members. AD subjects were all participants in a longitudinal research program maintained by the University of Pittsburgh, Alzheimer's Disease Research Center (ADRC). As participants in this program, patients underwent periodic neuropsychological and neurological evaluation. Clinical diagnosis of AD was based on a standardized ADRC evaluation at a Consensus Conference, utilizing DSM-IV [2] and NINCDS/ADRDA [14] criteria. Neuropathologic diagnosis was based, in part, on histologic examination of brain tissue sections with hematoxylin and eosin, thioflavine-S, and Bielschowsky silver stains. Each case received a severity rating of I–VI according to Braak and Braak [3]. Of the 17 cases, 3 cases were stage I, 1 was stage II, 1 was stage III, 3 were stage IV, there were no cases of stage V, and 9 were stage VI. Because of the small number of subjects within each stage, we grouped subjects into mild (stages I and II, $N=4$), moderate (stages III and IV, $N=4$), and severe (stages V and VI, $N=9$) groups. Of the 13 cases with a clinical diagnosis of AD, the number of subjects belonging to the mild, moderate, and severe groups was 0, 4, and 9, respectively. Likewise, the number of elderly controls belonging to these three groups was 4, 0, and 0, respectively. None of the patients had any other confounding neurological or neuropathologic disorders that interfered with our studies of the hippocampus.

Table 1

Number	Age	Sex	Weight (g)	PMI (h)	Braak stage
Non-demented subjects					
1	61	F	1360	18	I
2	57	F	1400	8	I
3	87	F	1120	8	I
4	88	F	990	5.5	II
AD subjects					
1	91	F	1260	3	III
2	75	M	1300	7	IV
3	81	M	1150	4	IV
4	72	M	1160	4	IV
5	100	F	970	5	VI
6	48	M	1100	8	VI
7	81	F	1130	4	VI
8	86	M	1330	2	VI
9	72	M	1080	4	VI
10	74	M	960	4	VI
11	62	M	1150	4	VI
12	84	F	1070	5	VI
13	89	F	1070	5	VI

Brain tissue was processed according to previously described procedures [9,10,15]. Blocks of tissue containing hippocampus were cut in a coronal plane and placed in 0.1 M phosphate buffer (PB, pH = 7.4) containing 4% paraformaldehyde for 24–48 h at 4 °C and then cryoprotected in 30% sucrose concentration in PB for several days. The tissue was then sectioned at 40 μm on a sliding, freezing microtome. For each case, at least one section was stained for Nissl substance to delineate the cytoarchitectural boundaries of the hippocampus as defined by Duvernoy [5].

The sections were processed for immunocytochemistry as previously described [9,10,15]. Tissue sections were immunocytochemically labeled using an avidin–biotin immunolabeled procedure using 4G8 and 2B2, both of which are raised in mice; 4G8 represents A2 while 2B2 represents B1 [11]. The primary antibodies were diluted 1/1000 for 4G8 and 1/2000 for 2B2 in Tris–saline containing 3% goat serum and 0.25% Triton X-100. At least three sections from each case were used for this study, and sections were processed together to control for any variability in the immunocytochemical procedure. As a control for nonspecific staining, sections were either incubated with initial incubation media minus the primary antibody or processed as described. Furthermore, representative sections were double-labeled using 4G8 or 2B2 and PHF-1 (generously provided by Dr. Peter Davis). PHF-1 recognizes tau protein phosphorylated at serine residues 396 and 404 [17]. Thus, these double-labeling studies allow us to investigate alterations of hnRNP A2 and B1 in neurons with NFT pathlogy. For double-labeling, immediately after the completion of PHF-1 immunohistochemistry, 4G8 or 2B2 immunohistochemistry was performed on the same section. As for chromagens, we used diaminobenzidine for PHF-1, and diaminobenzidine plus 2.5% nickel ammonium sulfate for 4G8 or 2B2, yielding brown and black reaction products, respectively.

Throughout the hippocampus intense A2 immunoreactivity was observed in the nucleoplasm of neurons and weak immunoreactivity was observed in the cytoplasm and proximal dendrites of neurons (Fig. 1A–L). A2 immunoreactivity was observed in the nucleoplasm of glial cells and ependymal cells, but the intensity was weak. In the subjects with mild pathology (Braak stages I and II), we observed an intense A2 immunoreactivity in the neuronal nucleoplasm from the CA3 to CA1 subfield (Fig. 1B–D), while CA4 neurons and the dentate granule cells were less intensely immunoreactive for A2 (Fig. 1A). In the moderately affected subjects (Braak stages III and IV), overall the distribution and intensity of A2 immunoreactivity appeared indistinguishable from that in mild cases (Fig. 1E–G), although the CA1 subfield showed a decrease in the number of A2 immunoreactive neurons and reduced A2 immunoreactivity in the remaining neurons (Fig. 1H). Interestingly, in the severely affected subjects (Braak stages V and VI), within the CA4 to CA2 subfields, the majority of neurons showed increased A2 immunoreac-

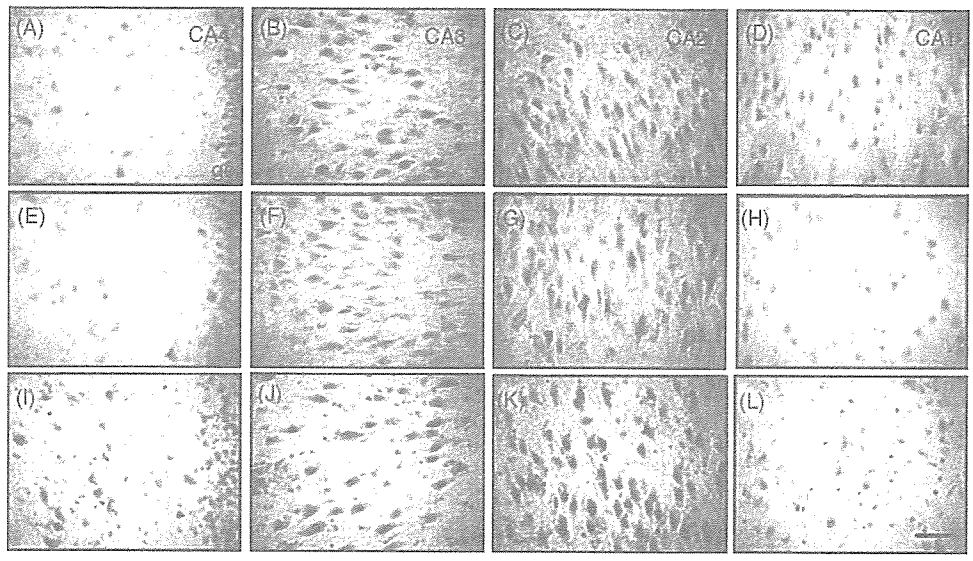

Fig. 1. Photomicrographs showing A2 immunohistochemistry in the hippocampus with mild (A–D), moderate (E–H), and severe (I–L) neurofibrillary pathology. In the mild case, an intense immunoreactivity for A2 was observed in the neuronal nucleoplasm from the CA3 to the CA1 subfield (B–D), while CA4 neurons and the dentate granule cells were less intensely immunoreactive (A). In the moderate case (E–G), overall the distribution and intensity of A2 immunoreactivity appeared indistinguishable from that in the mild cases, although the CA1 subfield showed a decrease in the number of A2 immunoreactive neurons and a reduction of A2 immunoreactivity in the remaining neurons (H). In the severely affected case, within the CA4 to CA2 subfields, the majority of neurons showed increased A2 immunoreactivity (I–K), while CA1 neurons maintained decreased A2 immunoreactivity (L). Bar = 50 μm. gc, granular cell.

tivity (Fig. 1I–K), while CA1 neurons maintained decreased A2 immunoreactivity (Fig. 1L).

In contrast to A2 immunoreactivity, immunoreactivity for B1 was observed exclusively in the nucleoplasm of neurons, in glial cells as well as ependymal cells, and it was not detected in the neuronal cytoplasm (Fig. 2A–L). An intense immunoreactivity for B1 was observed throughout the CA subfields, although in the granule cells, B1 immunoreactivity was relatively weak (Fig. 2A). In the moderately affected subjects, the pattern of B1 immunoreactivity was indistinguishable from that in the mild cases (Fig. 2E–G), although within the CA1 subfield we observed a decrease in the number of B1 immunoreactive neurons (Fig. 2H). In the severely affected subjects, within the CA4 to CA2 subfields neurons

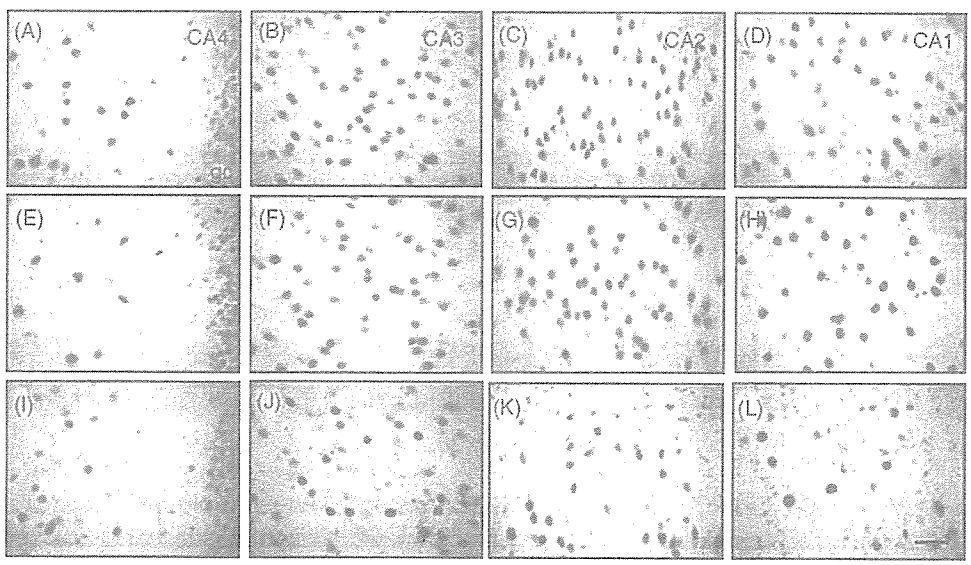

Fig. 2. Photomicrographs showing B1 immunohistochemistry in the hippocampus with mild (A–D), moderate (E–H), and severe (I–L), neurofibrillary pathology. In the mildly affected case, an intense immunoreactivity for B1 was observed throughout the CA subfields, although in the granule cells, B1 immunoreactivity was relatively weak (A). In the moderately affected case, the pattern of B1 immunoreactivity was indistinguishable from that in the mild cases (E–G), although within the CA1 subfield the number of B1 immunoreactive neurons was reduced (H). In the severely affected case, a decrease in B1 immunoreactivity was observed within the CA4 to CA2 subfields (I–K), and in the CA1 subfield, only a few neurons showed an intense immunoreactivity for B1 (L). Bar = 50 μm. gc, granular cell.

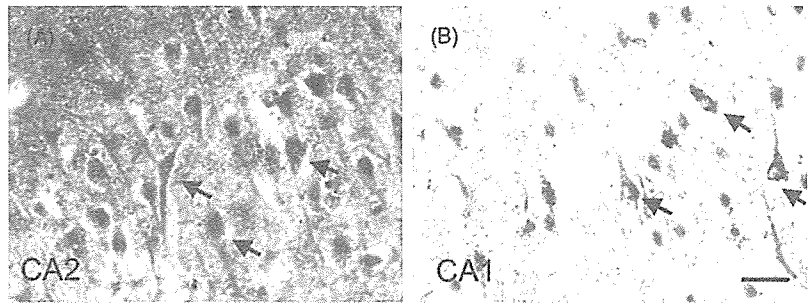

Fig. 3. Photomicrographs showing double-immunolabeling with PHF-1 (Fig. 2A and B, brown) and A2 (Fig. 2A, grey) or B1 (Fig. 2B, grey). PHF1-positive neurons often had reduced A2 and B1 immunoreactivity (black arrows). Bar = 50 μm.

often reduced B1 immunoreactivity (Fig. 2I–K), and in the CA1 subfield, only a few neurons showed immunoreactivity for B1 (Fig. 2L).

Double-immunolabeling study demonstrated that the majority of PHF1-positive neurons had reduced or lost A2 (Fig. 3A) and B1 (Fig. 3B) immunoreactivity, although we still observed intense immunoreactivity for A2 and B1 in some PHF1-positive neurons.

This is the first paper reporting A2 and B1 immunohistochemistry in the human hippocampus. Like our previous study on the rat brain and human neocortex, immunoreactivity for A2 and B1 was observed mainly in the nucleoplasm in neurons [9,10,15]. In the present study, we observed intense A2 and B1 immunoreactivity, although some variations in immunoreactivity were observed depending on the hippocampal regions. Since the intensity of immunoreactivity for these proteins may, in part, reflect post-transcriptional regulations, it is possible that in the human hippocampus, A2- and B1-associated post-transcription is highly activated, and post-trascriptional regulations associated with A2 and B1 are different from region to region.

In the AD hippocampus, we observed different alterations between A2 and B1. In the subjects with severe AD pathology, A2 immunoreactivity was increased in neurons within the CA fields except for CA1, while B1 immunoreactivity was decreased throughout the hippocampus. Interestingly, in our previous study, we observed increased A2 immunoreactivity and decreased B1 immunoreactivity in the hippocampal neurons 1, 3, 7, and 14 days after deafferentation of the perforant pathway on the rat brain [9]. The perforant pathway is well known as one of the most severely affected regions in the AD brain [8]. Thus, it is possible to suppose that alterations in A2 and B1 immunoreactivity observed in the AD hippocampus in the present study are in response to the deafferentation of the perforant pathway in the AD brain. Since A2 and B1 are produced by alternative splicing from a single copy gene [12], it is also possible that in response to AD pathology, neurons shift production from B1 to A2. It is documented that A2 has a function of mRNA trafficking in the neuronal dendrites as well as post-transcriptional regulation [20]. In line with this functional property of A2, we observed A2 immunoreactivity in the neuronal cytoplasm and proximal dendrites as well as in the nucleoplasm. In vitro study demonstrated that A2 binds many mRNAs localized in the dendrites, such as MAP2A, Arc, and GABA receptor α subunit [16]. In addition, neurons from CA4 to CA2 (i.e., the resistant zone) increased A2 but not in the CA1 subfield (i.e., the vulnerable zone). When these findings are taken together, it is plausible to suppose that neurons increase A2 to compensate for the dendritic damage in AD pathology.

In our previous study [10], we reported relative preservation of B1 immunoreactivity in the inferior temporal cortex of the AD brain. These observations appear inconsistent with the findings in the present study, that B1 immunolabeling decreased in the CA1 subregion in the moderately affected subjects, and in the severely affected cases, a decrease in B1 was observed in more extensive regions. One possible explanation for these inconsistent data is due to a difference of pathological severity between the hippocampus and the inferior temporal cortex. It is well known that AD pathology is much more severe in the hippocampus than in the neocortices. Thus, it is plausible to conclude that a decrease in B1 occurs in the advanced AD pathology.

We observed a decrease in A2 and B1 immunoreactivity in tangle-bearing neurons. Previous study demonstrated that total cellular RNA and polyadenylated RNA were substantially reduced in the AD cortex with neurofibrillary tangles [19]. In addition, the study of Ginsberg et al. [6] showed that tangle-bearing neurons reduced several classes of mRNAs that are known to encode proteins implicated in AD neuropathology. Although it remains to be determined whether post-transcriptional processes of these proteins are regulated by A2/B1, our study with double immunohistochemistry suggests that A2- and B1-associated post-transcriptional regulations are disturbed in NFT-bearing neurons.

Our study suggests that hnRNP A2 and B1 display a different response to AD pathology, with A2 being more resistant to AD pathology. The findings of increased A2 immunoreactivity in survival neurons in the resistant zone raise the possibility that neurons increase A2 in some compensatory mechanisms as a part of AD pathology. The double immunohistochemical studies suggest that A2- and B1-associated post-transcriptional regulations are disturbed in NFT- bearing neurons of the AD brain.

Acknowledgement

This work was supported by the Research Grant for Longevity Sciences (14C-4) from the Ministry of Health, Labour and Welfare.

References

[1] S. Akbarian, M.A. Smith, E.G. Jones, Editing for an AMPA receptor subunit RNA in prefrontal cortex and striatum in Alzheimer's disease, Huntington's disease and schizophrenia, Brain Res. 699 (1995) 297–304.

[2] American Psychiatric Association, Diagnostic and Statistical Manual of Mental Disorders, fourth ed., American Psychiatric Association, Washington, DC, 1994.

[3] H. Braak, E. Braak, Neuropathological staging of Alzheimer-related changes, Acta Neuropathol. (Berl.) 82 (1991) 239–259.

[4] G. Dreyfuss, M.J. Matunis, S. Piñol-Roma, C.G. Burd, HnRNP proteins and the biogenesis of mRNA, Annu. Rev. Biochem. 62 (1993) 289–321.

[5] H.M. Duvernoy, The Human Hippocampus, second ed, Springer-Verlag, Berlin, 1998.

[6] S.D. Ginsberg, S.E. Hemby, V.M. Lee, J.H. Eberwine, J.Q. Trojanowski, Expression profile of transcripts in Alzheimer's disease tangle-bearing CA1 neurons, Ann. Neurol. 48 (2000) 77–87.

[7] K. Honda, M.A. Smith, X. Zhu, D. Baus, W.C. Merrick, A.M. Tartakoff, T. Hattier, P.L. Harris, S.L. Siedlak, H. Fujioka, Q. Liu, P.I. Moreira, F.P. Miller, A. Nunomura, S. Shimohama, G. Perry, Ribosomal RNA in Alzheimer disease is oxidized by bound redox-active iron, J. Biol. Chem., March 14 (2005) (Epub. ahead of print).

[8] B.T. Hyman, G.W. Van Hoesen, A.R. Damasio, Alzheimer's disease: glutamate depletion in the hippocampal perforant pathway zone, Ann. Neurol. 22 (1987) 37–40.

[9] M. Ishikawa, K. Mizukami, M. Iwakiri, S. Hidaka, H. Kamma, T. Asada, Alterations of the hnRNP A2 and B1 in the hippocampus of the rat after perforant pathway lesion, Acta Neuropathol. (Berl.) 107 (2004) 144–148.

[10] M. Ishikawa, K. Mizukami, M. Iwakiri, H. Kamma, M.D. Ikonomovic, S.T. Dekosky, T. Asada, Immunohistochemical study of hnRNP B1 in the postmortem temporal cortices of patients with Alzheimer's disease, Neurosci. Res. 50 (2004) 481–484.

[11] H. Kamma, H. Satoh, M. Matsui, W.W. Wu, M. Fujiwara, H. Horiguchi, Characterization of hnRNP A2 and B1 using monoclonal antibodies: intracellular distribution and metabolism through cell cycle, Immunol. Lett. 76 (2001) 49–54.

[12] T. Kozu, B. Henrich, K.P. Schafer, Structure and expression of the gene (HNRPA2B1) encoding the human hnRNP protein A2/B1, Genomics 25 (1995) 365–371.

[13] S. Li, M. Mallory, M. Alford, S. Tanaka, E. Masliah, Glutamate transporter alterations in Alzheimer disease are possibly associated with abnormal APP expression, J. Neuropathol. Exp. Neurol. 56 (1997) 901–911.

[14] G. McKhann, D. Drachman, M. Folstein, R. Katzman, D. Price, E.M. Stadlan, Clinical diagnosis of Alzheimer's disease: report of the NINCDS-ADRDA Work Group under the auspices of Department of Health and Human Services Task Force on Alzheimer's Disease, Neurology 34 (1984) 939–944.

[15] K. Mizukami, H. Kamma, M. Ishikawa, G. Dreyfuss, Immunohistochemical study of the hnRNP A2 and B1 in the rat forebrain, NeuroReport 11 (2000) 3099–3102.

[16] T.P. Munro, R.J. Magee, G.J. Kidd, J.H. Carson, L. Bararese, L.M. Smith, R. Smith, Mutational analysis of a heterogeneous nuclear ribonucleoprotein A2 response element for RNA trafficking, J. Biol. Chem. 274 (1999) 34389–34395.

[17] L. Otvos Jr., L. Feiner, E. Lang, G.I. Szendrei, M. Goedert, V.M. Lee, Monoclonal antibody PHF-1 recognizes tau protein phosphorylated at serine residues 396 and 404, J. Neurosci. Res. 39 (1994) 669–673.

[18] S. Piñol Roma, G. Dreyfuss, Shuttling of premature mRNA bindings proteins between nucleus and cytoplasm, Nature 355 (1992) 730–732.

[19] E.M. Sajdel-Sulkowska, C.A. Marotta, Alzheimer's disease brain: alterations in RNA levels and in a ribonuclease-inhibitor complex, Science 225 (1984) 947–949.

[20] J. Shan, T.P. Munro, E. Barbarese, J.H. Carson, R. Smith, A molecular mechanism for mRNA trafficking in neuronal dendrites, J. Neurosci. 23 (2003) 8859–8866.

[21] W. Wallace, S.T. Ahlers, J. Gotlib, V. Bragin, J. Sugar, R. Gluck, P.A. Shea, K.L. Davis, V. Haroutunian, Amyloid precursor protein in the cerebral cortex is rapidly and persistently induced by loss of subcortical innervation, Proc. Natl. Acad. Sci. U.S.A. 90 (1993) 8712–8716.

[22] W.C. Wallace, V. Bragin, N.K. Robakis, K. Sambamurti, D. VanderPutten, C.R. Merril, K.L. Davis, A.C. Santucci, V. Haroutunian, Increased biosynthesis of Alzheimer amyloid precursor protein in the cerebral cortex of rats with lesions of the nucleus basalis of Meynert, Mol. Brain Res. 10 (1991) 173–178.

ELSEVIER

NeuroImage

www.elsevier.com/locate/ynimg
NeuroImage 28 (2005) 1014 – 1021

The prediction of rapid conversion to Alzheimer's disease in mild cognitive impairment using regional cerebral blood flow SPECT

Kentaro Hirao,[a,e] Takashi Ohnishi,[a,b,*] Yoko Hirata,[a] Fumio Yamashita,[a] Takeyuki Mori,[a] Yoshiya Moriguchi,[a] Hiroshi Matsuda,[a,f] Kiyotaka Nemoto,[a,d] Etsuko Imabayashi,[a,f] Minoru Yamada,[a,f] Toshihiko Iwamoto,[c] Kunimasa Arima,[c] and Takashi Asada[d]

[a]*Department of Radiology, National Center Hospital of Mental, Nervous, and Muscular Disorders, National Center of Neurology and Psychiatry, Tokyo, Japan*
[b]*Department of Investigative Radiology, Research Institute, National Cardiovascular Center, Osaka, Japan*
[c]*Department of Laboratory Medicine, National Center Hospital of Mental, Nervous, and Muscular Disorders, National Center of Neurology and Psychiatry, Tokyo, Japan*
[d]*Department of Psychiatry, Institute of Clinical Medicine, University of Tsukuba, Japan*
[e]*Department of Geriatric Medicine, Tokyo Medical University, Japan*
[f]*Department of Nuclear Medicine, Saitama Medical School, Japan*

Received 13 April 2005; revised 7 June 2005; accepted 30 June 2005
Available online 29 August 2005

Mild cognitive impairment (MCI) comprises a heterogeneous group with a variety of clinical outcomes and they are at risk for developing Alzheimer's disease (AD). The prediction of conversion from MCI to AD using the initial neuroimaging studies is an important research topic. We investigated the initial regional cerebral blood flow (rCBF) measurements using single photon emission computed tomography (SPECT) in individuals with 76 amnesic MCI (52 subjects converted to AD and 24 subjects did not convert to AD at 3-year follow-up) and 57 age- and gender-matched controls. We sought functional profiles associated with conversion to AD, then evaluated the predictive value of the initial rCBF SPECT. As compared with controls, AD converters demonstrated reduced blood flow in the bilateral parahippocampal gyri, precunei, posterior cingulate cortices, bilateral parietal association areas, and the right middle temporal gyrus. Non-converters also demonstrated significant reduction of rCBF in the posterior cingulated cortices and the right caudate nucleus when compared to controls. As compared with non-converters, converters showed reductions of rCBF in the bilateral temporo-parietal areas and the precunei. The logistic regression model revealed that reduced rCBF in the inferior parietal lobule, angular gyrus, and precunei has high predictive value and discriminative ability. Although a cross-validation study is needed to conclude the usefulness of rCBF SPECT for the prediction of AD conversion in individuals with MCI, our data suggest that the initial rCBF SPECT studies of individuals with MCI may be useful in predicting who will convert to AD in the near future.

Keywords: Mild cognitive impairment (MCI); Alzheimer's disease (AD); Regional cerebral blood flow (rCBF); Single photon emission computed tomography (SPECT)

Introduction

Mild cognitive impairment (MCI) is an operational diagnostic term developed to describe the preclinical stage of Alzheimer's disease (AD) (Petersen et al., 2001a). The risk for conversion to AD is higher in individuals with MCI than in the general aged population, as annual conversion rate of 6%–25% from MCI to AD (Petersen et al., 2001b). Furthermore, a recent study suggested that progression from MCI to AD is time-dependent. According to Palmer's study, people with MCI have a high risk of progressing to dementia over the next 3 years, and the risk starts to decrease after this point (Palmer et al., 2003). The early detection of MCI individuals who will later convert to AD is an important issue for both clinical and research interests.

The recent advance of computer-assisted statistical image analyses revealed that subjects with very mild AD typically show abnormal metabolic and regional cerebral blood flow (rCBF) patterns, even at the preclinical stage. Using glucose metabolism positron emission tomography (PET) with a voxel-by-voxel statistical analysis, Minoshima et al. reported that the earliest changes observed in very mild AD were in the posterior cingulate cortex (PCC) (Minoshima et al., 1997). This unexpected finding has

* Corresponding author. Department of Radiology, National Center Hospital of Mental, Nervous, and Muscular Disorders, National Center of Neurology and Psychiatry 4-1-1 Ogawa Higashi, Kodaira City, Tokyo 187-0031, Japan.
E-mail address: tohnishi@hotmail.com (T. Ohnishi).
Available online on ScienceDirect (www.sciencedirect.com).

1053-8119/$ - see front matter © 2005 Elsevier Inc. All rights reserved.
doi:10.1016/j.neuroimage.2005.06.066